Available online at www.sciencedirect.com
SCIENCE DIRECT®
International Journal of Solids and Structures 42 (2005) 1513–1535
INTERNATIONAL JOURNAL OF SOLIDS and STRUCTURES
www.elsevier.com/locate/ijsolstr

Green's functions for a bi-material problem with interfacial elliptical rigid inclusion and applications to crack and thin rigid line problems

P.B.N. Prasad [a,*], Norio Hasebe [a], X.F. Wang [a], Y. Shirai [b]

[a] *Department of Civil Engineering, Nagoya Institute of Technology, Gokiso-Cho, Showa-Ku, Nagoya 466, Japan*
[b] *Shizuoka Prefectural Government, Shizuoka, Japan*

Received 8 May 2004; received in revised form 11 July 2004
Available online 28 September 2004

Abstract

The Green's functions for a point force and dislocation interacting with interfacial elliptical rigid inclusion in a bonded bi-material system are obtained by applying complex variable method and conformal mapping technique. The problem of an internal crack or thin rigid line interacting with the interfacial inclusion is then examined. For mapping the half plane with a semi-elliptic notch a rational mapping function is used. This helps in evaluating certain contour integrals quite easily. The Green's function solutions are then used to simulate internal cracks or thin rigid lines to study their behavior in the presence of interfacial inclusion. Some interesting observations pertaining to the interaction between rigid inclusion and crack as well as between rigid inclusion and thin rigid line are discussed. In particular, stress intensity factors (SIF) at the tips of internal crack or stress singularity coefficients (SSC) at the tips of thin rigid line exhibit markedly different behavior depending on loading direction and distance between interfacial inclusion and crack (thin rigid line).
© 2004 Elsevier Ltd. All rights reserved.

Keywords: Green's functions; Bi-material; Rigid; Crack; Complex variable

1. Introduction

Interfaces in bi-materials and composites are sources to many defects like voids, cracks, inclusions that may appear during the processing or in service. The presence of such defects renders the interface weak and susceptible to failure under external loads. Several works examined the behavior of a crack or a void on a

* Corresponding author. Tel./fax: +81 52 735 5482.
E-mail address: bnprasad1@yahoo.com (P.B.N. Prasad).

0020-7683/$ - see front matter © 2004 Elsevier Ltd. All rights reserved.
doi:10.1016/j.ijsolstr.2004.07.014

bi-material interface due to external loads (Williams, 1959; Rice and Sih, 1965; Erdogan, 1965; England, 1965; Hasebe et al., 1990, 1992). Though there are some anomalies associated with interface crack problems, like oscillatory stress fields and crack face interpenetrations, they are confined to a small region surrounding the crack tip and can be neglected as shown by Rice (1988).

Anticracks or thin rigid lines are the counterpart of cracks and have singular stress fields near their tips similar to cracks. Mathematical treatment of cracks and thin rigid lines employing complex variable methods is similar. Dundurs and Markenscoff (1989) obtained Green's functions for thin rigid line problems by employing integral equation methods. Ballarini (1990) obtained the solution of a thin rigid line on a bi-material interface under remote loading while Markenscoff et al. (1994) solved the problem of an interfacial rigid line inclusion subjected to point forces and dislocations. Markenscoff and Ni (1996) also solved the problem of a debonded interfacial rigid line for remote loading case. Boniface and Hasebe (1998) studied the problem of an interface between two dissimilar half-planes and a rigid elliptic inclusion at the interface, and the degenerated case of thin rigid line was also considered. Though the singularities for crack and thin rigid line are same when they lie in a homogeneous medium, there are differences between the two. Rigid line solutions depend on Poisson's ratio whereas crack solutions do not, and their effects on the surrounding stress field are different. As noted by Ballarini (1990), interface crack and rigid line show dissimilarities and therefore a correspondence between the two problems should be made carefully.

Recently, many works focused on crack–inclusion interaction problems due to their importance in composites (Helsing, 1999; Cheesman and Santare, 2000; Theotokoglou and Theotokoglou, 2002; Hasebe et al., 2003a,b and references cited therein). The analysis of cracks ahead of inclusions or cavities is complicated by the fact that SIF can either increase or decrease depending on the elastic mismatch between the inclusion and the matrix. Hasebe et al. (2003b) have shown that for a crack ahead of a rigid rhombic or elliptical inclusion, SIF at the crack tips decrease as the distance between the inclusion and the crack decreases. On the other hand, a crack ahead of a hole of similar shape shows increasing SIF. It is important to note the dependence of rigid inclusion solutions on Poisson's ratio (v); changing v changes stress fields in the vicinity of the inclusion as also the SIF at crack tips.

The stresses ahead of a crack and of a thin rigid line reveal some interesting aspects. When a crack or rigid line lies in a homogeneous medium, stresses exhibit same singularity, viz. $1/\sqrt{r}$, where 'r' is the radial distance from the tip (Chen et al. (2003)). Whereas the crack singularity is due to loads normal to its plane, the rigid line singularity is due to loads both normal and parallel to its plane. Another feature is the absence of contribution of remote shear on the singular stresses at rigid line tip. However, it should be noted that load normal to a rigid line results in *negative* SSC at the tips; but the stress component perpendicular to the rigid line is still *positive*. Hasebe et al. (2003b) have shown that when a crack approaches rigid elliptical inclusion, SIF at crack tips decrease to zero. This could be attributed to the rigid boundary condition at the inclusion–matrix interface that results in the drop of SIF at the crack tips. By analyzing the stress fields in the vicinity of an interfacial rigid elliptical inclusion (Boniface and Hasebe, 1998), a rather different question is addressed in this paper: can a crack ahead of a rigid inclusion remain active (positive SIF at crack tips) when loading is parallel to the crack line and under what conditions?

In this paper, the Green's function of a point dislocation or point force interacting with an interfacial elliptical inclusion will be solved by employing complex variable methods and conformal mapping techniques. This solution will then be used to simulate an internal crack by the method of distributed dislocation technique or to simulate a thin rigid line by distributing point forces along the putative rigid line. The thin rigid line can rotate freely so that net forces and moments on the thin rigid line are zero. SIF at internal crack tips and SSC at internal rigid line tips are evaluated numerically by means of Gauss–Chebyshev quadrature (Erdogan et al., 1973; Chen and Hasebe, 1992). Several cases of crack and rigid line interacting with interfacial elliptical inclusion are considered. An interesting case of a crack ahead of inclusion and loading parallel to the crack line will be discussed. It is shown that such a crack can remain active (positive SIF) for specific loading and crack length.

2. Derivation of solution

The given problem consists of two half planes with different elastic properties, each containing a semi-elliptic rigid inclusion, bonded along the common boundary as shown in Fig. 1(a). Half plane occupying $Y \geqslant 0$ is designated as material 1 and $Y \leqslant 0$ as Material 2. Bi-material interface is denoted by M and rigid inclusion boundary by L_j where $j = 1,2$ correspond to materials 1 and 2, respectively. Shear modulus and Poisson's ratio for materials 1 and 2 are given by μ_j and v_j, respectively. Figs. 1(b) and (c) show the two half planes separately in z_1 and z_2 planes. The z_1 plane is obtained by rotating material 1 by 180° about X-axis while material 2 is undisturbed in the z_2 plane. Since the geometry of z_j planes are identical, same mapping function is used to map z_j planes onto unit circles as shown in Fig. 1(c). Regions inside and outside the unit circle are denoted by S^+ and S^-, respectively. Point dislocations $D_{01} = D_{X1} + iD_{Y1}$ and $-D_{01}$ are located in material 1 at z_{01} ($t_1 = t_{01}$) and at infinity ($t_1 = 1$), respectively. Dislocations, stresses and displacements in z_j planes are related to those in the original z-plane by

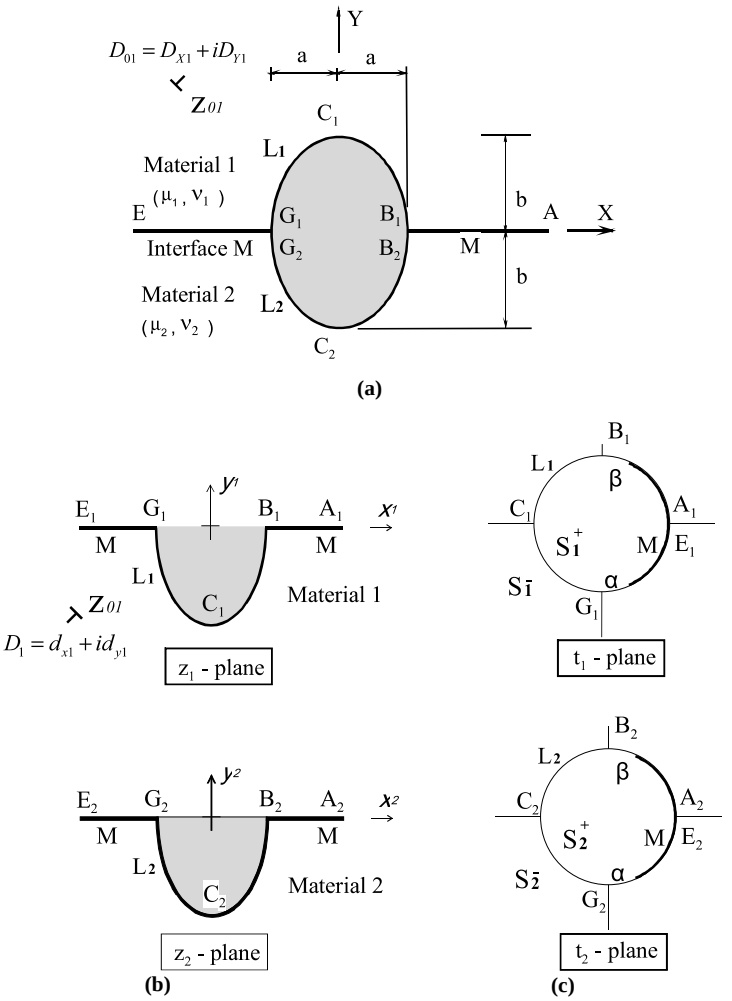

Fig. 1. (a) Dislocation interacting with interfacial elliptical rigid inclusion; (b) z_j plane (c) t_j plane.

$$\begin{aligned} &D_{X1} = -d_{x1} \quad D_{Y1} = d_{y1} \quad D_{X2} = d_{x2} \quad D_{Y2} = d_{y2} \\ &U_1 = u_1 \quad V_1 = -v_1 \quad U_2 = u_2 \quad V_2 = v_2 \\ &\sigma_{X1} = \sigma_{x1} \quad \sigma_{Y1} = \sigma_{y1} \quad \tau_{XY1} = -\tau_{xy1} \\ &\sigma_{X2} = \sigma_{x2} \quad \sigma_{Y2} = \sigma_{y2} \quad \tau_{XY2} = \tau_{xy2} \end{aligned} \tag{1}$$

The mapping function that maps a semi-elliptic notch onto a unit circle is given by

$$z_j = \omega(t_j) = \frac{E_0}{1 - t_j} + \sum_{k=1}^{N} \frac{E_k}{\zeta_k - t_j} + E_c, \quad j = 1, 2 \tag{2}$$

E_0, E_k, E_c, and ζ_k are complex constants and $N = 28$ in this analysis. The details of evaluating the constants in (2) are explained in Hasebe and Inohara (1980).

The solution for the given problem is solved in two stages: in the first stage (i) a point dislocation in a fixed half plane with a semi-elliptical notch (zero displacement condition) is solved (Fig. 1(b)); in the second stage (ii) the continuity conditions across the bonded part of the half planes are satisfied thus solving the problem completely. It should be noted that a similar procedure also applies if a point force instead of a dislocation acts in material 1. Accordingly, complex potentials for the upper half-plane (material 1) can be written in the mapped plane as

$$\begin{aligned} \phi_1(t_1) &= \phi_{1A}(t_1) + \phi_{d1}(t_1) \\ \psi_1(t_1) &= \psi_{1A}(t_1) + \psi_{d1}(t_1) \end{aligned} \tag{3}$$

where the suffix "d1" corresponds to the first stage (i) and suffix "1A" corresponds to the second stage (ii) mentioned above.

3. Half plane with an embedded semi-elliptic rigid inclusion (i)

The problem of a point dislocation in a half plane with an embedded semi-elliptic rigid inclusion (Fig. 1(b)) can be solved by a further subdivision into two basic problems: (a) point dislocation acting in an infinite homogeneous plane; (b) satisfying the fixed boundary conditions for the half plane with semi-elliptic inclusion. Thus the complex potential $\phi_{d1}(t_1)$ can be written as

$$\begin{aligned} \phi_{d1}(t_1) &= \phi_{d11}(t_1) + \phi_{d12}(t_1) \\ \psi_{d1}(t_1) &= \psi_{d11}(t_1) + \psi_{d12}(t_1) \end{aligned} \tag{4}$$

where the suffix 'd11' corresponds to infinite homogeneous plane consisting of the singular part of the solution while 'd12' corresponds to the regular solution ensuring the satisfaction of half plane boundary conditions.

The complex potentials for point dislocation acting at $z_{01}(t_{01})$ and $z_m(t_m)$ in an infinite plane are (Hasebe et al., 1996)

$$\begin{aligned} \phi_{d11}(t_1) &= -\frac{D_1}{2\pi}\{\log(t_1 - t_{01}) - \log(t_1 - t_m)\} \\ \psi_{d11}(t_1) &= -\frac{\overline{D_1}}{2\pi}\{\log(t_1 - t_{01}) - \log(t_1 - t_m)\} + \frac{D_1}{2\pi}\frac{\overline{\omega(t_{01})}}{\omega'(t_{01})(t_1 - t_{01})} - \frac{D_1}{2\pi}\frac{\overline{\omega(t_m)}}{\omega'(t_m)(t_1 - t_m)} \end{aligned} \tag{5}$$

Since the displacements are zero on the boundary,

$$\psi_{d1}(t_1) = \kappa_1 \overline{\phi_{d1}}(1/t_1) - \frac{\overline{\omega}(1/t_1)}{\omega'(t_1)}\phi'_{d1}(t_1) \tag{6}$$

or,

$$\psi_{d12}(t_1) = \kappa_1\overline{\phi_{d12}}(1/t_1) - \frac{\bar{\omega}(1/t_1)}{\omega'(t_1)}\phi'_{d12}(t_1) + \kappa_1\overline{\phi_{d11}}(1/t_1) - \frac{\bar{\omega}(1/t_1)}{\omega'(t_1)}\phi'_{d11}(t_1) - \psi_{d11}(t_1) \tag{6a}$$

Since $\psi_{d12}(t_1)$ is regular, the singular part on the right hand side of (6a) is equated to zero leading to

$$\begin{aligned}\overline{\phi_{d12}}(1/t_1) = &-\frac{\overline{D_1}}{2\pi\kappa_1}[\log(t_1 - t_{01}) - \log(t_1 - t_m)] \\ &+ \frac{D_1}{2\pi\kappa_1}\left[\frac{\overline{\omega(t_{01})} - \overline{\omega(1/\bar{t}_{01})}}{\omega'(t_{01})}\frac{1}{t_1 - t_{01}} - \frac{\overline{\omega(t_m)} - \overline{\omega(1/\overline{t_m})}}{\omega'(t_m)}\frac{1}{t_1 - t_m}\right] \\ &+ \frac{D_1}{2\pi\kappa_1}\sum_{k=1}^{N}\left(\frac{1}{\zeta'_k - t_m} - \frac{1}{\zeta'_k - t_{01}}\right)\frac{\overline{B_k}\zeta'^2_k}{t_1 - \zeta'_k} + \frac{1}{\kappa_1}\sum_{k=1}^{N}\frac{A_{d1k}\overline{B_k}\zeta'^2_k}{t_1 - \zeta'_k}\end{aligned}$$

where, $A_{d1k} \equiv \phi'_{d12}(\zeta'_k)$ and $B_k \equiv E_k/\overline{\omega'(\zeta'_k)}$. On taking the dislocation at z_m to infinity ($t_m = 1$), $\phi_{d12}(t_1)$ is obtained as

$$\begin{aligned}\phi_{d12}(t_1) = &-\frac{D_1}{2\pi\kappa_1}[\log(t_1 - t^*_{01}) - \log(t_1 - 1)] - \frac{\overline{D_1}}{2\pi\kappa_1}\left[\frac{\omega(t_{01}) - \omega(t^*_{01})}{\overline{\omega'(t_{01})}}\right]\frac{t^{*2}_{01}}{t_1 - t^*_{01}} \\ &- \frac{\overline{D_1}}{2\pi\kappa_1}\sum_{k=1}^{N}\left(\frac{1}{\overline{\zeta'_k} - 1} - \frac{1}{\overline{\zeta'_k} - \overline{t_{01}}}\right)\frac{B_k}{t_1 - \zeta_k} - \frac{1}{\kappa_1}\sum_{k=1}^{N}\frac{\overline{A_{d1k}}B_k}{t_1 - \zeta_k}\end{aligned} \tag{7}$$

where $t^*_{01} \equiv 1/\overline{t_{01}}$. $\phi_{d1}(t_1)$ is obtained from (4) while $\psi_{d1}(t_1)$ can be derived from (6). These complex potentials will now be used in conjunction with the continuity conditions across the interface to construct the solution for the bi-material problem (ii).

4. Solution for an elliptic rigid inclusion at a bi-material interface (ii)

The solution to the bi-material plane will now be constructed by ensuring the continuity of tractions and displacements across the interface. As the displacements are zero along the rigid elliptical inclusion boundary,

$$\kappa_j\phi_j(\sigma) - \frac{\omega(\sigma)}{\overline{\omega'(\sigma)}}\overline{\phi'_j(\sigma)} - \overline{\psi_j(\sigma)} = 0 \quad \text{on } L_j \tag{8}$$

where σ is a point on the unit circle in the mapped plane and is denoted by $\sigma = e^{i\theta}$. Hence, $\overline{\sigma} = 1/\sigma$ on the unit circle ($M + L_j$). Analytic continuation from zero displacement condition leads to

$$\psi_j(t_j) = \kappa_j\overline{\phi_j}(1/t_j) - \frac{\overline{\omega}(1/t_j)}{\omega'(t_j)}\phi'_j(t_j) \tag{9}$$

Substituting (9) into (8),

$$\phi^+_j(\sigma) - \phi^-_j(\sigma) = 0 \quad \text{on } L_j \tag{10}$$

where superscripts + and − denote the limiting values of the functions on the circumference when approached from inside and outside the unit circle, respectively.

Across the bonded interface 'M', traction and displacement continuity leads to

$$\phi^+_1(\sigma) + \kappa_1\phi^-_1(\sigma) = \overline{\phi^+_2(1/\overline{\sigma})} + \kappa_2\overline{\phi^-_2(1/\overline{\sigma})} \quad \text{on } M \tag{11}$$

$$\frac{\kappa_1}{\mu_1}\left[\phi_1^+(\sigma)-\phi_1^-(\sigma)\right]=\frac{\kappa_2}{\mu_2}\left[\overline{\phi_2^+(1/\overline{\sigma})}-\overline{\phi_2^-(1/\overline{\sigma})}\right]\quad\text{on } M \tag{12}$$

On writing

$$\phi_1(t_1)+\frac{\kappa_2\mu_1}{\kappa_1\mu_2}\overline{\phi_2(1/\overline{t_1})}=\Theta(t_1) \tag{13}$$

(12) can be written as

$$\Theta_1^+(\sigma)-\Theta_1^-(\sigma)=0 \tag{14}$$

General solution of (14) is an arbitrary rational function (Muskhelishvili, 1963)

$$\Theta(t_1)=\theta_1(t_1) \tag{15}$$

Since $\theta_1^+(\sigma)=\theta_1^-(\sigma)\equiv\theta_1(\sigma)$ on the boundary,

$$\overline{\phi_2^+(1/\overline{\sigma})}=\frac{\kappa_1\mu_2}{\kappa_2\mu_1}[-\phi_1^-(\sigma)+\theta_1(\sigma)] \tag{16a}$$

$$\overline{\phi_2^-(1/\overline{\sigma})}=\frac{\kappa_1\mu_2}{\kappa_2\mu_1}[-\phi_1^+(\sigma)+\theta_1(\sigma)] \tag{16b}$$

Substituting (16a, 16b) into (11), the boundary condition on M can be written as

$$\phi_1^+(\sigma)+A_1\phi_1^-(\sigma)=B_1\theta_1(\sigma) \tag{17}$$

$$A_1=\frac{\kappa_1}{\kappa_2}\left[\frac{\kappa_2\mu_1+\mu_2}{\kappa_1\mu_2+\mu_1}\right]=\left[\frac{(1+\alpha_D)-\Gamma(1+\beta_D)}{\Gamma\{-\Gamma(1-\alpha_D)+(1-\beta_D)\}}\right]\frac{(1-\beta_D)}{(1+\beta_D)}$$

$$B_1=\frac{\kappa_1\mu_2(\kappa_2+1)}{\kappa_2(\kappa_1\mu_2+\mu_1)}=\left[\frac{(1+\alpha_D)-\Gamma(1+\beta_D)}{-\Gamma(1-\alpha_D)+(1-\beta_D)}\right]\frac{(1-\alpha_D)}{(1+\beta_D)}$$

where α_D and β_D are the Dundurs parameters and $\Gamma=\mu_2/\mu_1$ given by

$$\alpha_D=\frac{(\kappa_1+1)\Gamma-(\kappa_2+1)}{(\kappa_1+1)\Gamma+(\kappa_2+1)},\quad \beta_D=\frac{(\kappa_1-1)\Gamma-(\kappa_2-1)}{(\kappa_1+1)\Gamma+(\kappa_2+1)}$$

By repeating the above procedure for $\phi_2(t_2)$, the following boundary condition on M can be formulated

$$\phi_2^+(\sigma)+A_2\phi_2^-(\sigma)=B_2\theta_2(\sigma) \tag{18}$$

$$A_2=\frac{\kappa_2}{\kappa_1}\left[\frac{\kappa_1\mu_2+\mu_1}{\kappa_2\mu_1+\mu_2}\right]=\left[\frac{\Gamma\{-\Gamma(1-\alpha_D)+(1-\beta_D)\}}{(1+\alpha_D)-\Gamma(1+\beta_D)}\right]\frac{(1+\beta_D)}{(1-\beta_D)}$$

$$B_2=\frac{\kappa_2\mu_1(\kappa_1+1)}{\kappa_1(\kappa_2\mu_1+\mu_2)}=\left[\frac{-\Gamma(1-\alpha_D)+(1-\beta_D)}{(1+\alpha_D)-\Gamma(1+\beta_D)}\right]\frac{(1+\alpha_D)}{(1-\beta_D)}$$

The problem of obtaining the potentials $\phi_1(t_1)$ and $\phi_2(t_2)$ is thus reduced to finding solutions to the Riemann–Hilbert (10), (17) and (18). Substituting (3) in (10) and (17) yields

$$\phi_{1A}^+(\sigma)-\phi_{1A}^-(\sigma)=0\quad\text{on } L_1 \tag{19}$$

$$\phi_{1A}^+(\sigma)+A_1\phi_{1A}^-(\sigma)=B_1\theta_{1A}(\sigma)+C_1\phi_{d1}(\sigma)\quad\text{on } M \tag{20}$$

where

$$C_1=-\mu_1(\kappa_1+1)/(\kappa_1\mu_2+\mu_1)=-(1+\alpha_D)/[\Gamma(1+\beta_D)]$$

and $\theta_{1A}(t_1) = \phi_{1A}(t_1) + (\kappa_2\mu_1/\kappa_1\mu_2)\overline{\phi_2(1/\bar{t}_1)}$ obtained by (13) and (15) is a rational function. Similarly,

$$\phi_2^+(\sigma) - \phi_2^-(\sigma) = 0 \quad \text{on } L_2 \tag{21}$$

$$\phi_2^+(\sigma) + A_2\phi_2^-(\sigma) = B_2\theta_{2A}(\sigma) + C_2\overline{\phi_{d1}(1/\bar{\sigma})} \quad \text{on } M \tag{22}$$

where

$$C_2 = \mu_2(\kappa_1 + 1)/(\kappa_2\mu_1 + \mu_2) = (1 + \alpha_D)/(1 - \beta_D)$$

and $\theta_{2A}(t_2) = \phi_2(t_2) + \overline{\phi_{1A}(1/\bar{t}_2)}$ is a rational function. The general solution to (19) and (20) can be written as (Muskhelishvili, 1963)

$$\phi_{1A}(t_1) = \frac{B_1\chi_1(t_1)}{2\pi\mathrm{i}}\int_M \frac{\theta_{1A}(\sigma)\mathrm{d}\sigma}{\chi_1^+(\sigma)(\sigma - t_1)} + \frac{C_1\chi_1(t_1)}{2\pi\mathrm{i}}\int_M \frac{\phi_{d1}(\sigma)\mathrm{d}\sigma}{\chi_1^+(\sigma)(\sigma - t_1)} + \chi_1(t_1)P_1(t_1) \tag{23}$$

where $P_1(t_1)$ is a rational function to be determined, $\chi_1(t_1) = (t_1 - \alpha)^{m_1}\ (t_1 - \beta)^{1-m_1}$, and $m_1 = 0.5 + \mathrm{i}(\log A_1)/2\pi$. The behavior of $\chi_1(t_1)$ is given by

$$\chi_1^+(\sigma) = -A_1\chi_1^-(\sigma) \quad \text{on } M$$

$$\chi_1^+(\sigma) = \chi_1^-(\sigma) \quad \text{on } L_1$$

Similarly, the general solution to (21) and (22) can be written as

$$\phi_2(t_2) = \frac{B_2\chi_2(t_2)}{2\pi\mathrm{i}}\int_M \frac{\theta_{2A}(\sigma)\mathrm{d}\sigma}{\chi_2^+(\sigma)(\sigma - t_2)} + \frac{C_2\chi_2(t_2)}{2\pi\mathrm{i}}\int_M \frac{\overline{\phi_{d1}(1/\bar{\sigma})}\mathrm{d}\sigma}{\chi_2^+(\sigma)(\sigma - t_2)} + \chi_2(t_2)P_2(t_2) \tag{24}$$

where $P_2(t_2)$ is also a rational function to be determined, $\chi_2(t_2) = (t_2 - \alpha)^{m_2}(t_2 - \beta)^{1-m_2}$, and $m_2 = 0.5 + \mathrm{i}(\log A_2)/2\pi$.

The second term in (23) and (24) is evaluated using the residue theorem as

$$\begin{aligned}
&\frac{C_1\chi_1(t_1)}{2\pi\mathrm{i}}\int_M \frac{\phi_{d1}(\sigma)}{\chi_1^+(\sigma)(\sigma - t_1)}\mathrm{d}\sigma \\
&= \frac{C_1\chi_1(t_1)}{2\pi\mathrm{i}(1 + A_1)}\oint_M \frac{\phi_{d1}(\sigma)}{\chi_1(\sigma)(\sigma - t_1)}\mathrm{d}\sigma \\
&= \frac{C_1}{2\pi(1 + A_1)}\left[-\frac{D_1}{\kappa_1}\left\{\log(t_1 - t_{01}^*) - \log(t_1 - 1) + \chi_1(t_1)\int_{t_{01}^*}^1 \frac{\mathrm{d}\sigma}{\chi_1(\sigma)(\sigma - t_1)}\right\}\right. \\
&\quad - D_1\left\{\log(t_1 - t_{01}) - \log(t_1 - 1) + \chi_1(t_1)\int_{t_{01}}^1 \frac{\mathrm{d}\sigma}{\chi_1(\sigma)(\sigma - t_1)}\right\} \\
&\quad - \frac{\overline{D_1}}{\kappa_1}\frac{\omega(t_{01}) - \omega(t_{01}^*)}{\overline{\omega'(t_{01})}}\left[1 - \frac{\chi_1(t_1)}{\chi_1(t_{01}^*)}\right]\frac{t_{01}^{*2}}{t_1 - t_{01}^*} \\
&\quad - \frac{\overline{D_1}}{\kappa_1}\sum_{k=1}^N\left(\frac{1}{\overline{\zeta_k'} - 1} - \frac{1}{\overline{\zeta_k'} - \overline{t_{01}}}\right)\left[1 - \frac{\chi_1(t_1)}{\chi_1(\zeta_k)}\right]\frac{B_k}{t_1 - \zeta_k} \\
&\quad \left. - \frac{2\pi}{\kappa_1}\sum_{k=1}^N \frac{\overline{A_{d1k}}B_k}{t_1 - \zeta_k}\left[1 - \frac{\chi_1(t_1)}{\chi_1(\zeta_k)}\right]\right]
\end{aligned} \tag{25}$$

$$\frac{C_2\chi_2(t_2)}{2\pi \mathrm{i}}\int_M \frac{\overline{\phi_{d1}(1/\overline{\sigma})}}{\chi_2^+(\sigma)(\sigma-t_2)}\mathrm{d}\sigma$$

$$=\frac{C_2\chi_2(t_2)}{2\pi \mathrm{i}(1+A_2)}\oint_M \frac{\overline{\phi_{d1}(1/\overline{\sigma})}}{\chi_2(\sigma)(\sigma-t_2)}\mathrm{d}\sigma$$

$$=\frac{C_2}{2\pi(1+A_2)}\left[-\overline{D_1}\left\{\log(t_2-t_{01}^*)-\log(t_2-1)+\chi_2(t_2)\int_{t_{01}^*}^1 \frac{\mathrm{d}\sigma}{\chi_2(\sigma)(\sigma-t_2)}\right\}\right.$$

$$-\frac{\overline{D_1}}{\kappa_1}\left\{\log(t_2-t_{01})-\log(t_2-1)+\chi_2(t_2)\int_{t_{01}}^1 \frac{\mathrm{d}\sigma}{\chi_2(\sigma)(\sigma-t_2)}\right\}$$

$$+\frac{D_1}{\kappa_1}\frac{\overline{\omega(t_{01})}-\overline{\omega(t_{01}^*)}}{\omega'(t_{01})}\left[1-\frac{\chi_2(t_2)}{\chi_2(t_{01})}\right]\frac{1}{t_2-t_{01}}$$

$$+\frac{D_1}{\kappa_1}\sum_{k=1}^N\left(\frac{1}{\zeta_k'-1}-\frac{1}{\zeta_k'-t_{01}}\right)\left[1-\frac{\chi_2(t_2)}{\chi_2(\zeta_k')}\right]\frac{B_k\zeta_k'^2}{t_2-\zeta_k'}$$

$$\left.+\frac{2\pi}{\kappa_1}\sum_{k=1}^N\frac{A_{d1k}\overline{B_k}\zeta_k'^2}{t_2-\zeta_k'}\left[1-\frac{\chi_2(t_2)}{\chi_2(\zeta_k')}\right]\right] \tag{26}$$

The contour integrals of (25) and (26) are carried out as outlined in Hasebe et al. (1991). Also, the first derivatives of the integral terms in (25) and (26) can be expressed by terms without integrals (Hasebe et al. (1991)).

The rational function $\theta_{1A}(t_1)$ can be expressed as a sum of irregular terms inside and outside the unit circle as

$$\theta_{1A}(t_1)=\sum_n \frac{a_{1n}}{\xi_{1n}-t_1}+\sum_n \frac{b_{1n}}{\eta_{1n}-t_1} \tag{27}$$

where $|\xi_{1n}|>1$, $|\eta_{1n}|<1$, and a_{1n} and b_{1n} are complex constants to be determined. Substituting (27) into (23) the first term is evaluated using residue theorem as

$$\frac{B_1\chi_1(t_1)}{2\pi \mathrm{i}}\int_M \frac{\theta_{1A}(\sigma)\mathrm{d}\sigma}{\chi_1^+(\sigma)(\sigma-t_1)}$$

$$=\frac{B_1\chi_1(t_1)}{2\pi \mathrm{i}(1+A_1)}\oint_M \frac{\theta_{1A}(\sigma)\mathrm{d}\sigma}{\chi_1(\sigma)(\sigma-t_1)}$$

$$=\frac{B_1}{1+A_1}\left\{\sum_n\left[1-\frac{\chi_1(t_1)}{\chi_1(\xi_{1n})}\right]\frac{a_{1n}}{\xi_{1n}-t_1}+\sum_n\left[1-\frac{\chi_1(t_1)}{\chi_1(\eta_{1n})}\right]\frac{b_{1n}}{\eta_{1n}-t_1}\right\} \tag{28}$$

$P_1(t_1)$ is obtained from the regularity of $\psi_{1A}(t_1)$. Substituting (3) into (7),

$$\psi_{1A}(t_1)=\kappa_1\overline{\phi_{1A}}(1/t_1)-\frac{\overline{\omega}(1/t_1)}{\omega'(t_1)}\phi_{1A}'(t_1)+\kappa_1\overline{\phi_{d1}}(1/t_1)-\frac{\overline{\omega}(1/t_1)}{\omega'(t_1)}\phi_{d1}'(t_1)-\psi_{d1}(t_1) \tag{29}$$

From (23), (25) and (28), the first term in (29) can be written as

$$\overline{\phi_{1A}}(1/t_1)=\overline{\chi_1}(1/t_1)\overline{P_1}(1/t_1)+\text{terms regular in } S_1^+$$

The second term in (29) can expressed as

$$\frac{\overline{\omega}(1/t_1)}{\omega'(t_1)}\phi'_{1A}(t_1) = -\sum_{k=1}^{N}\frac{A_{1k}\overline{B_k}\zeta'^2_k}{\zeta'_k - t_1} + \text{terms regular in } S^+$$

where $A_{1k} \equiv \phi'_{1A}(\zeta'_k)$. From (6), the last three terms on the right hand side of (29) disappear.

Thus, $\psi_{1A}(t_1)$ is written as

$$\psi_{1A}(t_1) = \kappa_1\overline{\chi_1}(1/t_1)\overline{P_1}(1/t_1) + \sum_{k=1}^{N}\frac{A_{1k}\overline{B_k}\zeta'^2_k}{\zeta'_k - t_1} + \text{terms regular in } S^+$$

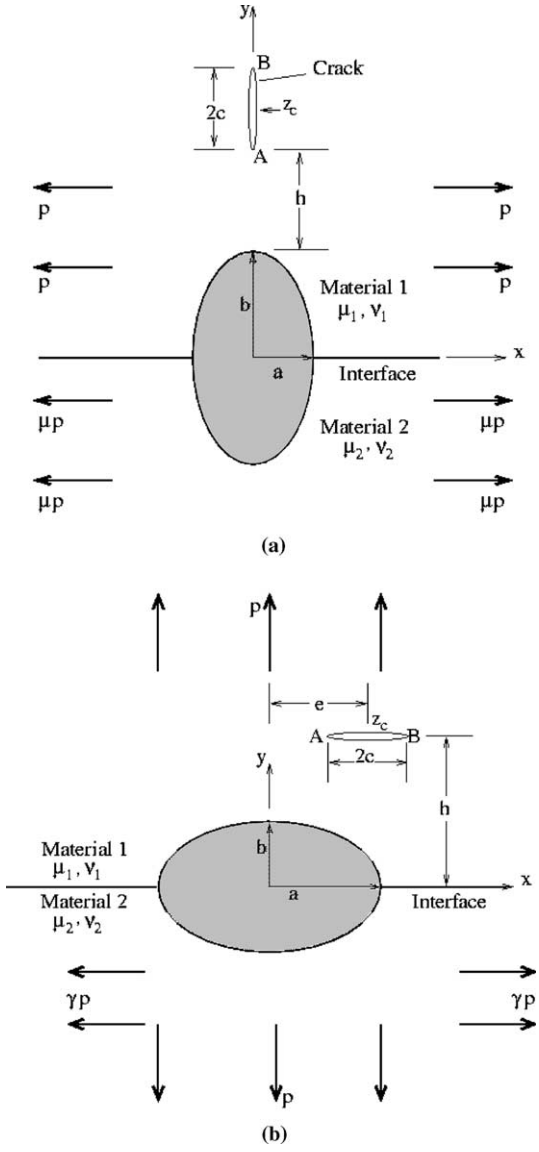

Fig. 2. Loading (a) parallel to and (b) normal to bi-material interface.

Since $\psi_{1A}(t_1)$ is regular in S^+, the irregular part should be cancelled out. Expanding the first term in Laurent series and equating terms with pole at $t_1 = \zeta'_k$ to zero, we get

$$P_1(t_1) = \frac{1}{\kappa_1}\sum_{k=1}^{N}\frac{\overline{A_{1k}}B_k}{\chi_1(\zeta_k)(\zeta_k - t_1)} \tag{30}$$

Similarly, $P_2(t_2)$ can be obtained as

$$P_2(t_2) = \frac{1}{\kappa_2}\sum_{k=1}^{N}\frac{\overline{A_{2k}}B_k}{\chi_2(\zeta_k)(\zeta_k - t_2)} \tag{31}$$

In order to evaluate the function $\Theta_1(t_1)$, the following relations are used:

$$\frac{\overline{\chi_2(1/\overline{t_1})}}{\overline{\chi_2(1)}} = \frac{\chi_1(t_1)}{t_1\chi_1(1)}, \quad \frac{\overline{\chi_2(1/\overline{t_1})}}{\overline{\chi_2(\xi_{2n})}} = \frac{\xi'_{2n}\chi_1(t_1)}{t_1\chi_1(\xi'_{2n})}, \quad \frac{\overline{\chi_2(1/\overline{t_1})}}{\overline{\chi_2(\eta_{2n})}} = \frac{\eta'_{2n}\chi_1(t_1)}{t_1\chi_1(\eta'_{2n})}$$

where $\xi'_{2n} \equiv 1/\overline{\xi_{2n}}$, $\eta'_{2n} \equiv 1/\overline{\eta_{2n}}$, $A_2 = 1/A_1$, and $m_2 = \overline{m_1}$. Using (23) and (24)

$$\begin{aligned}
\theta_{1A}(t_1) &= \phi_{1A}(t_1) + \overline{\phi_2(1/\overline{t_1})} \\
&= \frac{B_1}{1+A_1}\left\{\sum_n\left[1 - \frac{\chi_1(t_1)}{\chi_1(\xi_{1n})}\right]\frac{a_{1n}}{\xi_{1n} - t_1} + \sum_n\left[1 - \frac{\chi_1(t_1)}{\chi_1(\eta_{1n})}\right]\frac{b_{1n}}{\eta_{1n} - t_1}\right\} \\
&\quad - \frac{B_2}{1+A_2}\frac{\kappa_2\mu_1}{\kappa_1\mu_2}\left\{\sum_n\left[1 - \frac{\chi_1(t_1)}{\chi_1(\eta'_{2n})}\right]\frac{\overline{b_{2n}}\eta'^2_{2n}}{\eta'_{2n} - t_1} + \sum_n\left[1 - \frac{\chi_1(t_1)}{\chi_1(\xi'_{2n})}\right]\frac{\overline{a_{2n}}\xi'^2_{2n}}{\xi'_{2n} - t_1}\right\} \\
&\quad + \frac{1}{\kappa_1}\sum_{k=1}^{N}\frac{\chi_1(t_1)\overline{A_{1k}}B_k}{\chi_1(\zeta_k)(\zeta_k - t_1)} - \frac{\kappa_2\mu_1}{\kappa_1\mu_2}\sum_{k=1}^{N}\frac{\chi_1(t_1)A_{2k}\overline{B_k}\zeta'^2_k}{\chi_1(\zeta'_k)(\zeta'_k - t_1)}
\end{aligned} \tag{32}$$

Since (27) and (32) are identical, their poles must be the same and the coefficients in the two terms, which either include or exclude the Plemelj functions, must also be equal at each pole in S_1^+ and S_1^-. Therefore, the coefficients are evaluated as

$$\begin{aligned}
&\xi_{1k} = \eta'_{2k} = \zeta_k, \quad a_{1k} = -\overline{A_{1k}}B_k, \quad a_{2k} = -\overline{A_{2k}}B_k, \\
&\eta_{1k} = \xi'_{2k} = \zeta'_k, \quad b_{1k} = A_{2k}\overline{B_k}\zeta'^2_k, \quad b_{2k} = A_{1k}\overline{B_k}\zeta'^2_k
\end{aligned}$$

Thus,

$$\theta_{1A}(t_1) = -\sum_{k=1}^{N}\frac{\overline{A_{1k}}B_k}{\zeta_k - t_1} + \sum_{k=1}^{N}\frac{A_{2k}\overline{B_k}\zeta'^2_k}{\zeta'_k - t_1} \tag{33}$$

Finally, $\phi_{1A}(t_1)$ is obtained as

$$\begin{aligned}
\phi_{1A}(t_1) &= \frac{B_1}{\kappa_1(1+A_1)}\sum_{k=1}^{N}\left[1 + \frac{1 + A_1 - B_1}{B_1}\frac{\chi_1(t_1)}{\chi_1(\zeta_k)}\right]\frac{\overline{A_{1k}}B_k}{\zeta_k - t_1} - \frac{B_1}{\kappa_1\Gamma(1+A_1)}\sum_{k=1}^{N}\left[1 - \frac{\chi_1(t_1)}{\chi_1(\zeta'_k)}\right]\frac{A_{2k}\overline{B_k}\zeta'^2_k}{\zeta'_k - t_1} \\
&\quad + \frac{C_1}{2\pi(1+A_1)}\left[-\frac{D_1}{\kappa_1}\left\{\log(t_1 - t^*_{01}) - \log(t_1 - 1) + \chi_1(t_1)\int_{t^*_{01}}^{1}\frac{\mathrm{d}\sigma}{\chi_1(\sigma)(\sigma - t_1)}\right\}\right. \\
&\quad \left. - D_1\left\{\log(t_1 - t_{01}) - \log(t_1 - 1) + \chi_1(t_1)\int_{t_{01}}^{1}\frac{\mathrm{d}\sigma}{\chi_1(\sigma)(\sigma - t_1)}\right\}\right. \\
&\quad - \frac{\overline{D_1}}{\kappa_1}\frac{\omega(t_{01}) - \omega(t^*_{01})}{\overline{\omega'(t_{01})}}\left[1 - \frac{\chi_1(t_1)}{\chi_1(t^*_{01})}\right]\frac{t^{*2}_{01}}{t_1 - t^*_{01}} - \frac{\overline{D_1}}{\kappa_1}\sum_{k=1}^{N}\left(\frac{1}{\overline{\zeta'_k} - 1} - \frac{1}{\overline{\zeta'_k} - \overline{t_{01}}}\right) \\
&\quad \left. \times\left[1 - \frac{\chi_1(t_1)}{\chi_1(\zeta_k)}\right]\frac{B_k}{t_1 - \zeta_k} - \frac{2\pi}{\kappa_1}\sum_{k=1}^{N}\frac{\overline{A_{d1k}}B_k}{t_1 - \zeta_k}\left[1 - \frac{\chi_1(t_1)}{\chi_1(\zeta_k)}\right]\right]
\end{aligned} \tag{34}$$

The complex potentials in the final form can be written as

$$\phi_1(t_1) = \phi_{1A}(t_1) + \phi_{d1}(t_1) \tag{35}$$

$$\begin{aligned}\phi_2(t_2) = {} & \frac{B_2}{\kappa_2(1+A_2)} \sum_{k=1}^{N} \left[1 + \frac{1+A_2-B_2}{B_2} \frac{\chi_2(t_2)}{\chi_2(\zeta_k)}\right] \frac{\overline{A_{2k}} B_k}{\zeta_k - t_2} - \frac{\Gamma B_2}{\kappa_2(1+A_2)} \sum_{k=1}^{N} \left[1 - \frac{\chi_2(t_2)}{\chi_2(\zeta_k')}\right] \frac{A_{1k}\overline{B_k}\zeta_k'^2}{\zeta_k' - t_2} \\ & + \frac{C_2}{2\pi(1+A_2)} \left[-\overline{D_1} \left\{ \log(t_2 - t_{01}^*) - \log(t_2 - 1) + \chi_2(t_2) \int_{t_{01}^*}^{1} \frac{\mathrm{d}\sigma}{\chi_2(\sigma)(\sigma - t_2)} \right\} \right. \\ & - \frac{\overline{D_1}}{\kappa_1} \left\{ \log(t_2 - t_{01}) - \log(t_2 - 1) + \chi_2(t_2) \int_{t_{01}}^{1} \frac{\mathrm{d}\sigma}{\chi_2(\sigma)(\sigma - t_2)} \right\} \\ & + \frac{D_1}{\kappa_1} \frac{\overline{\omega(t_{01})} - \overline{\omega(t_{01}^*)}}{\omega'(t_{01})} \left[1 - \frac{\chi_2(t_2)}{\chi_2(t_{01})}\right] \frac{1}{t_2 - t_{01}} + \frac{D_1}{\kappa_1} \sum_{k=1}^{N} \left(\frac{1}{\zeta_k' - 1} - \frac{1}{\zeta_k' - t_{01}} \right) \left[1 - \frac{\chi_2(t_2)}{\chi_2(\zeta_k')}\right] \frac{B_k \zeta_k'^2}{t_2 - \zeta_k'} \\ & \left. + \frac{2\pi}{\kappa_1} \sum_{k=1}^{N} \frac{A_{d1k}\overline{B_k}\zeta_k'^2}{t_2 - \zeta_k'} \left[1 - \frac{\chi_2(t_2)}{\chi_2(\zeta_k')}\right] \right] \end{aligned} \tag{36}$$

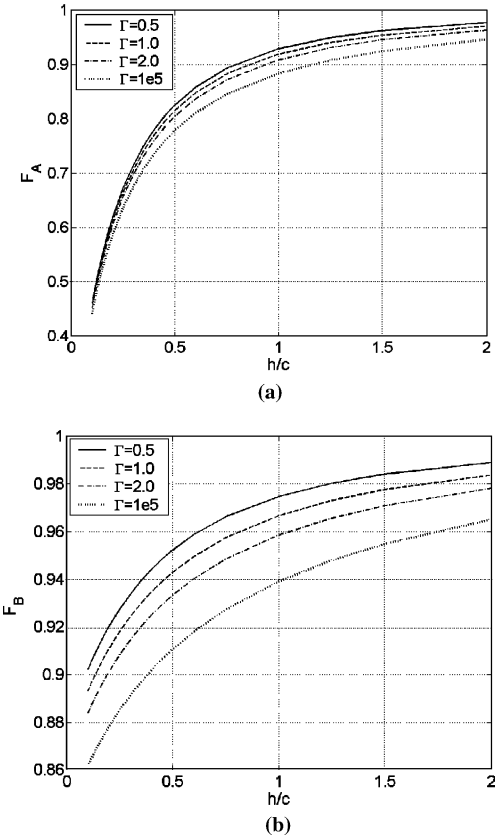

Fig. 3. Normalized SIF of an internal crack interacting with interfacial circular rigid inclusion (load parallel to the interface): (a) crack tip A, (b) crack tip B ($a/b = 1$, $a/c = 1$, $b/c = 1$; $\kappa_1 = \kappa_2 = 2$; $F_{A,B} = K_{A,B}/p\sqrt{\pi c}$).

where $A_{1k} \equiv \phi'_{1A}(\zeta'_k)$, $A_{2k} \equiv \phi'_2(\zeta'_k)$. The first derivatives of $\phi_1(t_1)$ and $\phi_2(t_2)$ do not involve integral terms present in (35) and (36). Hence, numerical integration is not necessary to calculate A_{1k} and A_{2k} as well as stress components. However, numerical integration is necessary to compute displacements as they involve both the complex potentials and their derivatives. The complex constants A_{1k} and A_{2k} ($k = 1, 2, \ldots, N$) are determined by solving the $4N$ simultaneous linear equations corresponding to the real and imaginary parts of A_{1k} and A_{2k}. The complex potentials $\psi_j(t_j)$ ($j = 1, 2$) are given by (7).

The Green's function for a point force q_1 at t_{01} and $-q_1$ at $t_m = 1$ ($z_m = \infty$) in the t_1-plane interacting with an interfacial elliptical rigid inclusion can be obtained by adopting a similar procedure outlined for point dislocation above. The complex potentials for the half-planes are

$$\phi_1(t_1) = \phi_{1A}(t_1) + \phi_{q11}(t_1) + \phi_{q12}(t_1) \tag{37}$$

where

$$\phi_{q11}(t_1) = \frac{q_1}{2\pi}[\log(t_1 - t_{01}) - \log(t_1 - 1)] \tag{38}$$

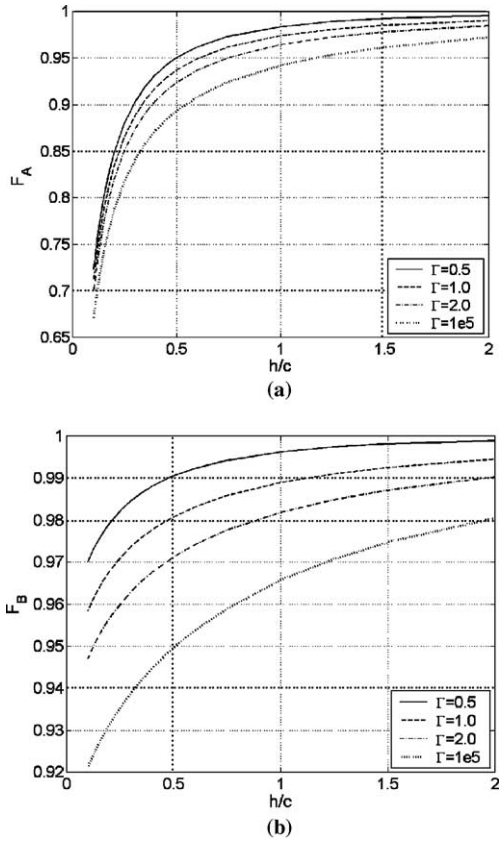

Fig. 4. Normalized SIF of an internal crack interacting with interfacial elliptical rigid inclusion (load parallel to the interface): (a) crack tip A, (b) crack tip B ($a/b = 0.5$, $a/c = 0.5$, $b/c = 1$; $\kappa_1 = \kappa_2 = 2$; $F_{A,B} = K_{A,B}/p\sqrt{\pi c}$).

$$\phi_{q12}(t_1) = \frac{1}{2\pi}\left\{-q_1[\log(t_1 - t_{01}^*) - \log(t_1 - 1)] + \frac{\overline{q_1}}{\kappa_1}\left[\frac{\omega(t_{01}) - \omega(t_{01}^*)}{\overline{\omega'(t_{01})}}\right]\frac{t_{01}^{*2}}{t_1 - t_{01}^*} + \frac{\overline{q_1}}{\kappa_1}\sum_{k=1}^{N}\left(\frac{1}{\overline{\zeta_k'} - 1} - \frac{1}{\overline{\zeta_k'} - \overline{t_{01}}}\right)\frac{B_k}{t_1 - \zeta_k} - \frac{2\pi}{\kappa_1}\sum_{k=1}^{N}\frac{\overline{A_{q1k}}B_k}{t_1 - \zeta_k}\right\} \tag{39}$$

$$\phi_{1A}(t_1) = \frac{B_1}{\kappa_1(1 + A_1)}\sum_{k=1}^{N}\left[1 + \frac{1 + A_1 - B_1}{B_1}\frac{\chi_1(t_1)}{\chi_1(\zeta_k)}\right]\frac{\overline{A_{1k}}B_k}{\zeta_k - t_1} - \frac{B_1}{\kappa_1\Gamma(1 + A_1)}\sum_{k=1}^{N}\left[1 - \frac{\chi_1(t_1)}{\chi_1(\zeta_k')}\right]\frac{A_{2k}\overline{B_k}\zeta_k'^2}{\zeta_k' - t_1} + \frac{C_1}{2\pi(1 + A_1)}\left[q_1\left\{\log(t_1 - t_{01}) - \log(t_1 - t_{01}^*) + \chi_1(t_1)\int_{t_{01}}^{t_{01}^*}\frac{\mathrm{d}\sigma}{\chi_1(\sigma)(\sigma - t_1)}\right\} + \frac{\overline{q_1}}{\kappa_1}\frac{\omega(t_{01}) - \omega(t_{01}^*)}{\overline{\omega'(t_{01})}}\left[1 - \frac{\chi_1(t_1)}{\chi_1(t_{01}^*)}\right]\frac{t_{01}^{*2}}{t_1 - t_{01}^*} + \frac{\overline{q_1}}{\kappa_1}\sum_{k=1}^{N}\left(\frac{1}{\overline{\zeta_k'} - 1} - \frac{1}{\overline{\zeta_k'} - \overline{t_{01}}}\right)\left[1 - \frac{\chi_1(t_1)}{\chi_1(\zeta_k)}\right]\frac{B_k}{t_1 - \zeta_k} - \frac{2\pi}{\kappa_1}\sum_{k=1}^{N}\frac{\overline{A_{q1k}}B_k}{t_1 - \zeta_k}\left[1 - \frac{\chi_1(t_1)}{\chi_1(\zeta_k)}\right]\right] \tag{40}$$

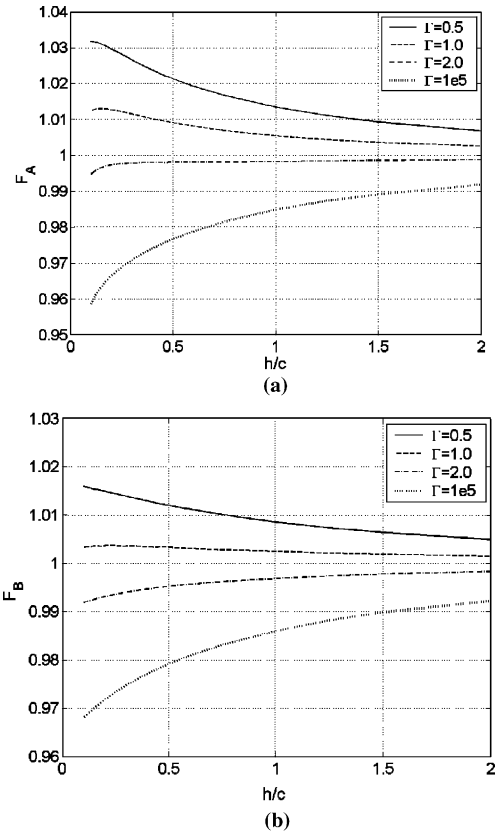

Fig. 5. Normalized SIF of an internal crack interacting with interfacial thin rigid line inclusion (load parallel to the interface): (a) crack tip A, (b) crack tip B ($a/b = 0$, $a/c = 0$, $b/c = 1$; $\kappa_1 = \kappa_2 = 2$; $F_{A,B} = K_{A,B}/p\sqrt{\pi c}$).

where $A_{q1k} \equiv \phi'_{q12}(\zeta'_k)$, and

$$\phi_2(t_2) = \frac{B_2}{\kappa_2(1+A_2)} \sum_{k=1}^{N} \left[1 + \frac{1+A_2-B_2}{B_2} \frac{\chi_2(t_2)}{\chi_2(\zeta_k)}\right] \frac{\overline{A_{2k}} B_k}{\zeta_k - t_2} - \frac{\Gamma B_2}{\kappa_2(1+A_2)} \sum_{k=1}^{N} \left[1 - \frac{\chi_2(t_2)}{\chi_2(\zeta'_k)}\right] \frac{A_{1k}\overline{B_k}\zeta'^2_k}{\zeta'_k - t_2}$$
$$+ \frac{C_2}{2\pi(1+A_2)} \left[\overline{q_1}\left\{\log(t_2 - t^*_{01}) - \log(t_2 - t_{01}) + \chi_2(t_2)\int_{t^*_{01}}^{t_{01}} \frac{\mathrm{d}\sigma}{\chi_2(\sigma)(\sigma - t_2)}\right\}\right.$$
$$- \frac{q_1}{\kappa_1} \frac{\overline{\omega(t_{01})} - \overline{\omega(t^*_{01})}}{\omega'(t_{01})} \left[1 - \frac{\chi_2(t_2)}{\chi_2(t_{01})}\right] \frac{1}{t_2 - t_{01}} - \frac{q_1}{\kappa_1} \sum_{k=1}^{N} \left(\frac{1}{\zeta'_k - 1} - \frac{1}{\zeta'_k - t_{01}}\right) \left[1 - \frac{\chi_2(t_2)}{\chi_2(\zeta'_k)}\right] \frac{B_k \zeta'^2_k}{t_2 - \zeta'_k}$$
$$\left. + \frac{2\pi}{\kappa_1} \sum_{k=1}^{N} \frac{A_{q1k}\overline{B_k}\zeta'^2_k}{t_2 - \zeta'_k} \left[1 - \frac{\chi_2(t_2)}{\chi_2(\zeta'_k)}\right]\right] \tag{41}$$

where $A_{1k} \equiv \phi'_{1A}(\zeta'_k)$, $A_{2k} \equiv \phi'_2(\zeta'_k)$. It should be noted that although there is a replacement formula between the stress functions of point dislocation and point force for homogeneous material problem (Hasebe et al., 2003b), the same procedure cannot be carried out directly for bi-material problem because of the differences of the forms of stress functions: (36) contains term $\log(t_1 - 1)$ whereas (41) does not. In the next section, the Green's functions obtained above will be used to simulate an internal crack or a thin rigid line to study their behaviors in the presence of interfacial elliptical rigid inclusion under arbitrary remote loads.

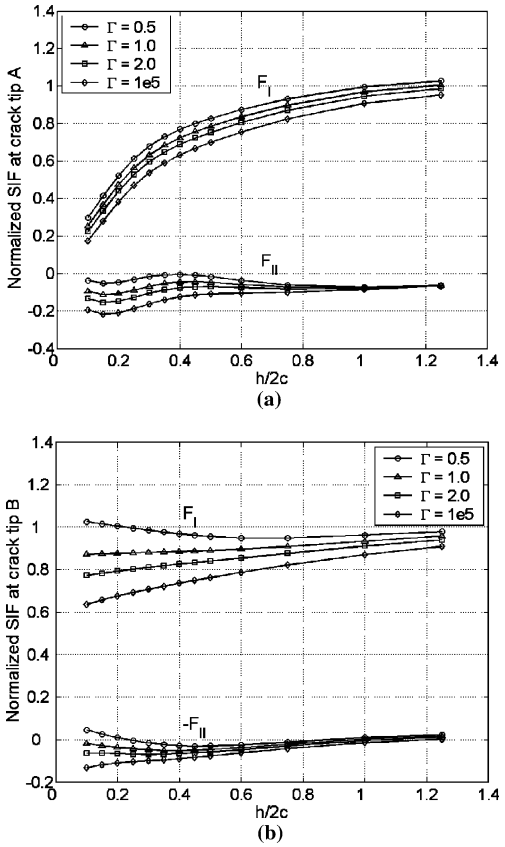

Fig. 6. Normalized SIF of an internal crack interacting with interfacial circular rigid inclusion (load normal to the interface): (a) crack tip A, (b) crack tip B ($b/a = 1$, $a/c = 1$, $b/c = 1$, $e/c = 2$; $\kappa_1 = \kappa_2 = 2$; $F_{\mathrm{I,II}} = K_{\mathrm{I,II}}/p\sqrt{\pi c}$).

5. Results

5.1. Internal crack

The numerical procedure for simulating an internal crack or thin rigid line using dislocations and point forces is well known and will not be elucidated here. Details of the numerical procedure can be found in Erdogan et al. (1973) and Chen and Hasebe (1992). Simulations are carried out for various shapes of interfacial inclusion and internal crack (thin rigid line) orientations and varying the distance between them.

The problem of an internal crack interacting with an interfacial rigid elliptical inclusion and subjected to remote loads will be considered first. Remote loading parallel and normal to the bi-material interface are considered as shown in Fig. 2(a) and (b), respectively. The values of μ and γ in Fig. 2 are given by $(1+\alpha_D)/(1-\alpha_D)$ and $2(2\beta_D-\alpha_D)/(1-\alpha_D)$, respectively (Boniface and Hasebe (1998)). Length of the internal crack is denoted by "$2c$" and the separation distance between the elliptical inclusion and crack tip A is "h". For loading normal to the interface (Fig. 2(b)), internal crack is offset by an amount "e".

The solution for an interfacial rigid elliptical inclusion subjected to remote loads has been obtained by Boniface and Hasebe (1998) and will be used in conjunction with the Green's functions obtained in the preceding section. The numerical procedure is carried out using Gauss–Chebyshev quadrature and

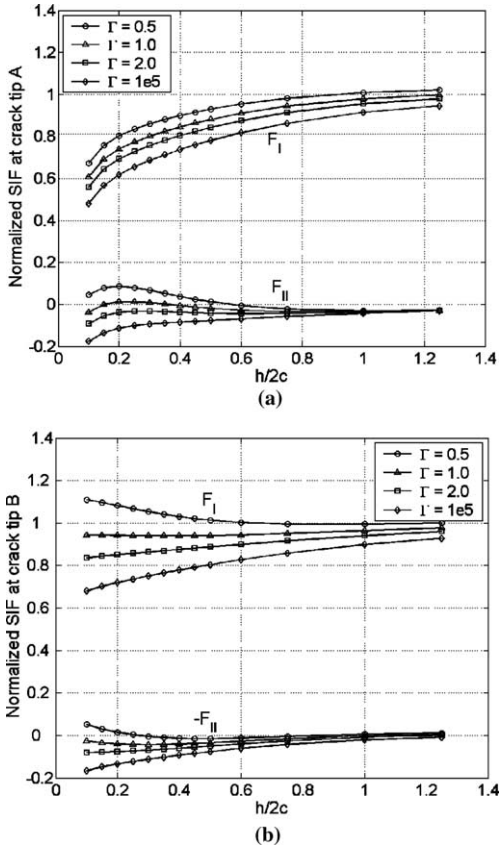

Fig. 7. Normalized SIF of an internal crack interacting with interfacial elliptical rigid inclusion (load normal to the interface): (a) crack tip A, (b) crack tip B ($b/a=0.5$, $a/c=1$, $b/c=0.5$, $e/c=2$; $\kappa_1=\kappa_2=2$; $F_{I,II}=K_{I,II}/p\sqrt{\pi c}$).

the accuracy of the computed results is within 0.01. In all the cases considered in this paper, Muskhelishvili's constant κ_j is taken as 2 for both the materials 1 and 2.

Fig. 3 shows the variation of normalized SIF at internal crack tips with the separation distance "*h*/*c*" for loading parallel to the interface. It can be seen that SIF at crack tip A decreases as "h" decreases (Fig. 3(a)). This decrease can be attributed to the rigid boundary conditions on the inclusion boundary. Similar trend in SIF can be noticed for other inclusion shapes shown in Fig. 4 for rigid elliptic inclusion whereas Fig. 5 for thin rigid line penetrating through the interface has a different trend: the values of SIF for both tips A and B are divergent to some extent as the crack approaches the rigid line. But the SIF at crack tip B reaches a finite value. The results for crack tip A suggest that it is difficult for a crack to penetrate rigid inclusion since SIF at tip A drop to zero as the separation distance decreases. Hasebe et al. (2003b) obtained similar results for an internal crack interacting with a rigid rhombic inclusion in a homogeneous medium. In contrast, for an internal crack approaching an interfacial cavity, SIF at tip A becomes unbounded as the distance "*h*" decreases as shown by Prasad et al. (2004a,b). This implies that it is difficult for a crack to penetrate inclusion as it becomes harder. The decrease in SIF at internal crack tips is more when the inclusion shape is circular and less as the ellipse dimension "*a*" decreases. This can be attributed to the effect of inclusion shape on the range of dominance of its stress field; this range is more for circular inclusion and decreases as one of the ellipse dimensions decreases. A similar but opposite effect can be noticed for an

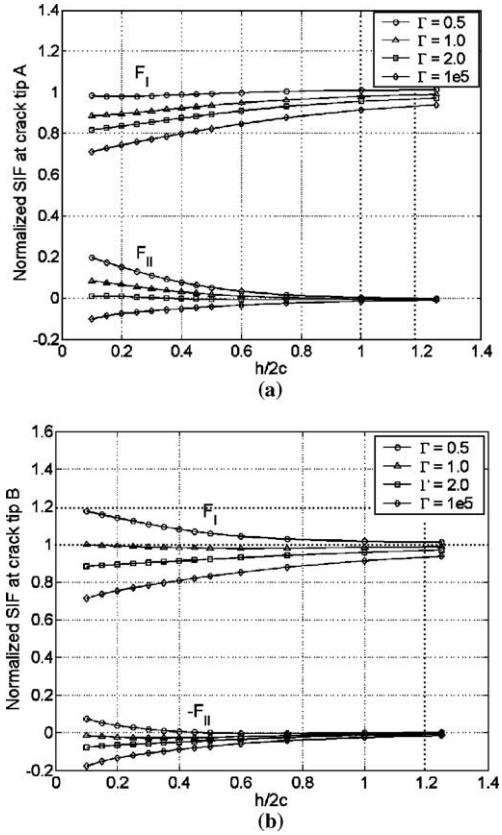

Fig. 8. Normalized SIF of an internal crack interacting with interfacial rigid line inclusion (load normal to the interface): (a) crack tip A, (b) crack tip B ($b/a = 0$, $a/c = 1$, $b/c = 0$, $e/c = 2$; $\kappa_1 = \kappa_2 = 2$; $F_{\mathrm{I,II}} = K_{\mathrm{I,II}}/\pi c$).

interfacial elliptical hole where SIF increases at the internal crack tips and is more for circular hole shape when compared other shapes as shown by Prasad et al. (2004b).

Fig. 6 shows normalized SIF at crack tips A and B when the remote load is normal to the interface (see Fig. 2(b)). SIF at crack tip A decreases with "h" similar to the cases discussed above. However, there is a mode-II component as well which is absent when the load is parallel to the interface. This can be attributed to the symmetry of loading and geometry in the latter case. Similar trends in SIF variation are seen for other inclusion shapes considered as shown in Fig. 7 (elliptical inclusion with major axis along the interface) and Fig. 8 (interfacial thin rigid line). Again, the drop in SIF at the internal crack tips is more for circular

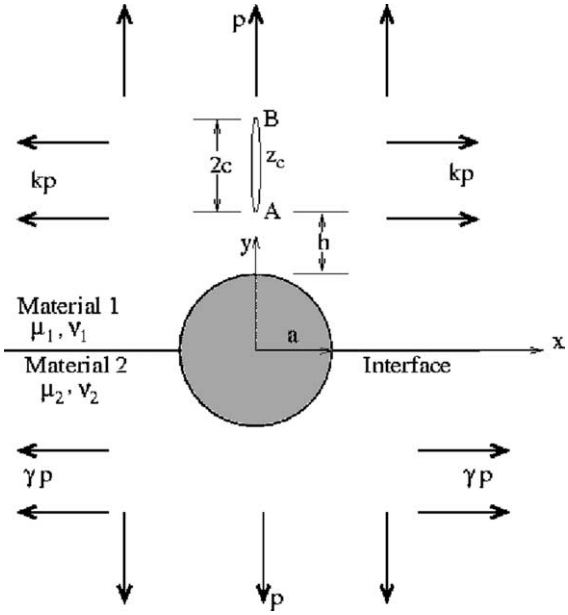

Fig. 9. Internal crack interacting with interfacial circular rigid inclusion subjected to bi-axial loading; $-1 \leqslant k \leqslant 1$ and $\gamma = [k + \alpha_D(k-2) + 4\beta_D]/(1-\alpha_D)$.

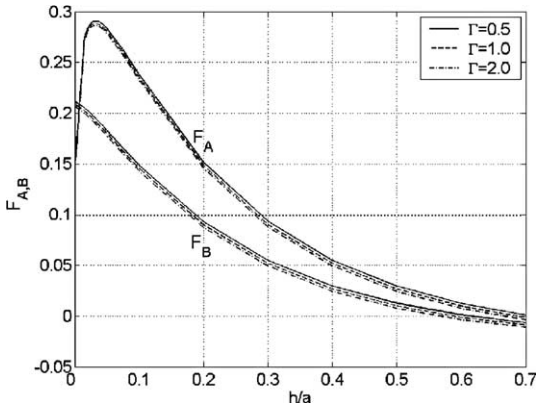

Fig. 10. Normalized SIF of an internal crack interacting with interfacial rigid circular inclusion (load parallel to the crack line) ($k = 0$; $a/b = 1$, $a/c = 10$, $b/c = 1$; $\kappa_1 = \kappa_2 = 2$; $F_{A,B} = K_{A,B}/p\sqrt{\pi c}$).

inclusion when compared to other inclusion shapes. It should be noted that in all the cases considered above, loading is normal to the internal crack line.

An interesting case of remote load parallel to the internal crack will be considered. From conventional fracture mechanics point of view such a load has no influence on cracks, i.e., SIF at the crack tips is zero. It will be shown that when an internal crack lies ahead of a rigid inclusion, cracks can remain active (positive SIF at the crack tips) even though the applied load is parallel to the crack. Fig. 9 shows an internal crack

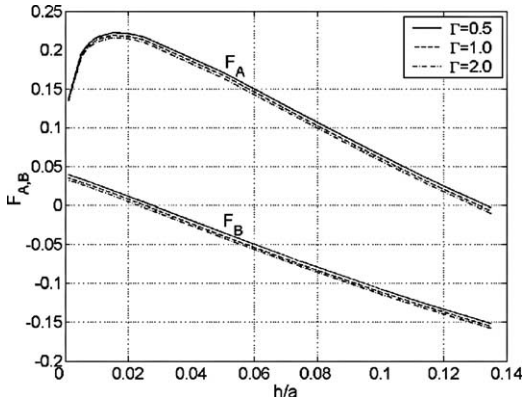

Fig. 11. Normalized SIF of an internal crack interacting with interfacial rigid circular inclusion (load parallel to the crack line) ($k = -0.5$; $a/b = 1$, $a/c = 10$, $b/c = 10$; $\kappa_1 = \kappa_2 = 2$; $F_{A,B} = K_{A,B}/p\sqrt{\pi c}$).

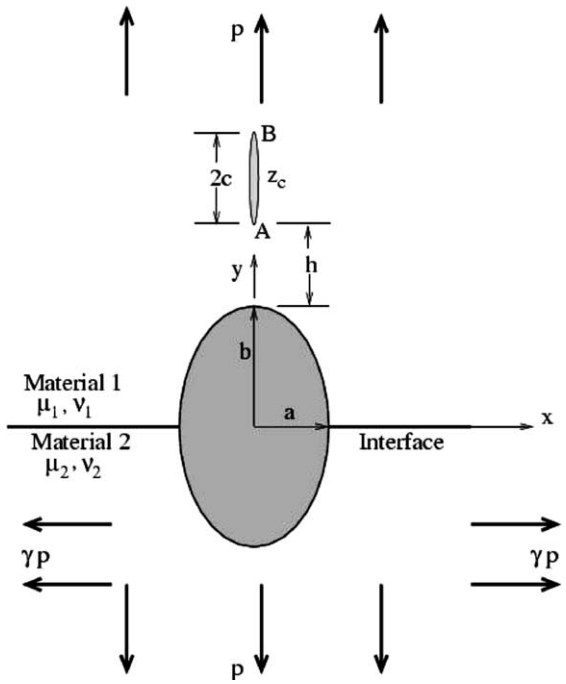

Fig. 12. Internal thin rigid line interacting with interfacial elliptical rigid inclusion.

ahead of an interfacial rigid circular inclusion subjected to bi-axial remote loading. Load normal to the interface is "p" while the load parallel to the interface is "kp" where $-1 \leqslant k \leqslant 1$. By adjusting the value of "k" desired bi-axial load can be achieved. The value of multiplying "p" in material 2 (Fig. 9) is $k\mu + \gamma$ (see Fig. 2(a) and (b)) and is given by $\gamma = [k + \alpha_D(k-2) + 4\beta_D]/(1-\alpha_D)$. With reference to Fig. 9, Boniface and Hasebe (1998) have shown that the normal stress component (σ_{xx}), along y-axis, ahead of an interfacial rigid inclusion remains positive when the applied remote load is normal to the interface i.e., $k = 0$. The extent of this region (positive σ_{xx}) depends on material mismatch and Poisson's ratio of materials 1 and 2. This suggests that if an internal crack lies in the region where σ_{xx} remains positive, the crack tips can have positive SIF (active crack).

Fig. 10 shows the variation in SIF of an internal crack subjected to uni-axial load parallel to the crack ($k = 0$). It should be noted that internal crack size for this case adjusted such that it lies in the region of positive σ_{xx} discussed above ($a/c = b/c = 10$). It can be seen that crack tips A and B are active (positive mode-I). An interesting aspect of variation in SIF of crack tip A is the initial increase up to a certain "h/a" after which it decreases again. Whereas the decrease in SIF as the crack approaches the rigid inclusion is due to the rigid boundary conditions on the inclusion boundary, the initial increase in SIF is due to

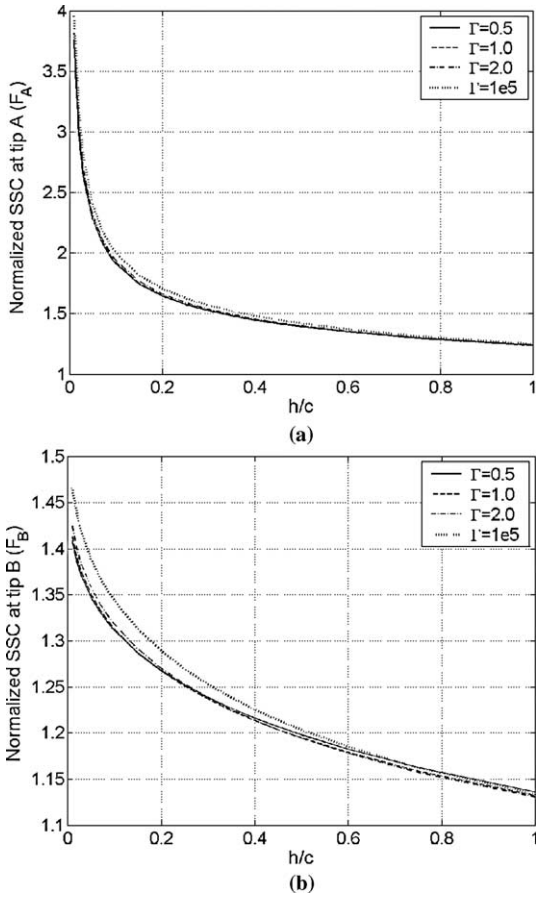

Fig. 13. Normalized SSC of a thin rigid line interacting with interfacial rigid circular inclusion (load parallel to the rigid line) ($a/b = 1$, $a/c = 1$, $b/c = 1$; $\kappa_1 = \kappa_2 = 2$; $F_{A,B} = [4\kappa_1/(1+\kappa_1)]K_{A,B}/p\sqrt{\pi c}$).

increasing σ_{xx} as the inclusion boundary is approached (Fig. 9). Thus, there is a competition between increasing SIF due to increasing σ_{xx} (along y-axis) and decreasing SIF due to rigid boundary conditions on the inclusion boundary. Eventually, rigid boundary conditions prevail thus decreasing the SIF at crack tip A. It should be noted that the range of positive σ_{xx} varies with elastic mismatch and Poisson's ratio; this range may be negligible for certain combinations of Poisson's ratio and elastic mismatch and can be easily shown from the results of Boniface and Hasebe (1998).

Another interesting bi-axial loading situation is considered that is commonly ignored in conventional fracture mechanics. For this case, load normal to the crack line is compressive ($k = -0.5$) as shown in Fig. 9. Fig. 11 shows that SIF at crack tip A is positive for the range of "h" considered. The variation of SIF at tip A is similar to the previous case of uni-axial load parallel to the crack. However, SIF at crack tip B varies from positive to negative as "h" increases indicating crack closure. This is due to part of the crack (crack tip B) lying in the compressive σ_{xx} field. For $h/a \leqslant 0.025$, SIF at both the tips A and B are positive. The range of bi-axial loading ratio "k" for which crack ahead of interfacial inclusion can remain active is not taken up here; but, it suffices to state here that "k", "κ_j" and "μ_j" decide whether a crack ahead of an interfacial rigid inclusion remains active in addition to the requirement that the internal crack lie within the zone where normal stress to the crack line is positive. This also explains the possibility of the presence of micro-cracks ahead of inclusions for loading cases that were hitherto neglected.

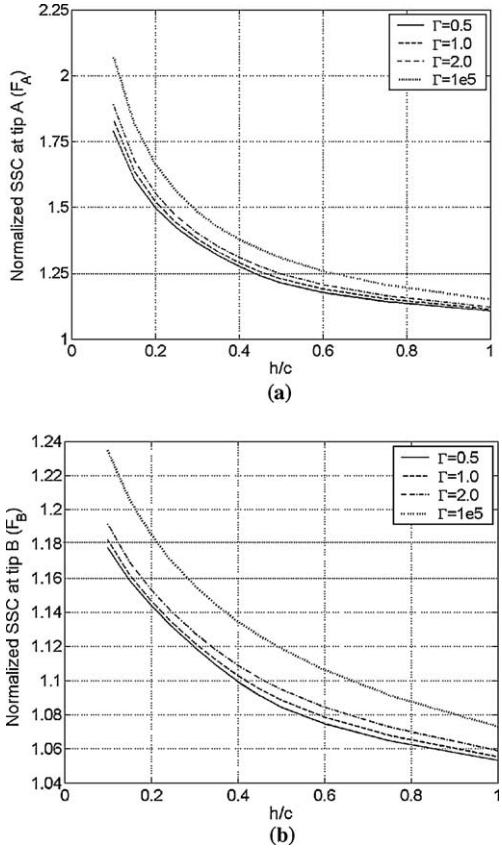

Fig. 14. Normalized SSC of a thin rigid line interacting with interfacial rigid line inclusion (load parallel to the rigid line) ($a/b = 0$, $a/c = 0$, $b/c = 1$; $\kappa_1 = \kappa_2 = 2$; $F_{A,B} = [4\kappa_1/(1+\kappa_1)]K_{A,B}/p\sqrt{\pi c}$).

5.2. Thin rigid line

The problem of a rigid line inclusion and multiple rigid line inclusions subjected to remote loads as well as first and second order singularities has been analyzed by several authors (Hasebe and Takeuchi, 1985; Dundurs and Markenscoff, 1989; Cheung and Chen, 1989; Ballarini, 1990; Chen and Hasebe, 1992; Markenscoff et al., 1994; Markenscoff and Ni, 1996). Hasebe et al. (1988) examined the problem of a partially debonded semi-elliptic rigid inclusion embedded in a half-plane by using rational mapping technique. Boniface and Hasebe (1998) studied the problem of a rigid elliptical inclusion on a bi-material interface subjected to remote loading. It should be noted that a line inclusion is a special case of an elliptical inclusion. Despite their mathematically similar treatment, line inclusions and cracks are dissimilar in many respects. A compilation of results on rigid line problems can be found in Murakami et al. (1992).

In this section, a rigid line inclusion interacting with an interfacial rigid elliptical inclusion will be considered. The numerical treatment of a rigid line inclusion can be found in Chen and Hasebe (1992) and will not be elaborated here. The geometry of the problem is shown in Fig. 12. Separation distance between the interfacial elliptical inclusion and thin rigid line is denoted by "h". Load is applied parallel to the rigid line inclusion as shown in Fig. 12. Fig. 13 shows the normalized stress singularity coefficient (SSC) for a rigid

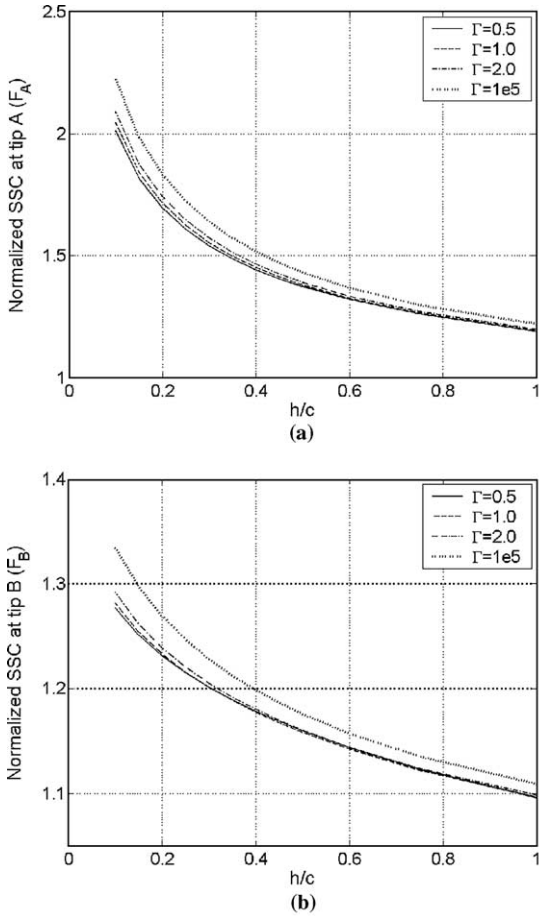

Fig. 15. Normalized SSC of a thin rigid line interacting with interfacial rigid elliptical inclusion (load parallel to the rigid line) ($a/b = 0.5$, $a/c = 0.5$, $b/c = 1$; $\kappa_1 = \kappa_2 = 2$; $F_{A,B} = [4\kappa_1/(1+\kappa_1)]K_{A,B}/p\sqrt{\pi c}$).

line interacting with interfacial rigid circular inclusion. As the separation distance decreases, SSC at tip A becomes unbounded while at tip B it remains bounded. In contrast, for an internal crack, SIF at tip A tends to zero as "h" decreases. The singularity at the rigid line tips suggest the possibility of cracks initiating from the tips or debonding of rigid line from the matrix. Similar trends can be found for other inclusion shapes. Figs 14 and 15 show normalized SSC of an internal thin rigid line interacting with a rigid line penetrating the bi-material interface and an interfacial rigid elliptical inclusion, respectively. It can be seen that the SSC at tip A increases significantly as the distance "h" decreases for all the cases considered. It should be noted that, unlike a crack, a thin rigid line cannot propagate and as such concepts like energy release rate cannot be used. But the singularity at the rigid line tip may lead to crack initiation from rigid line tips or debonding of rigid lines. When the applied remote load is normal to the rigid line a negative SSC is obtained. It should be emphasized that negative SSC at rigid line tips does not imply that the rigid line is inactive. For a rigid line in a homogeneous medium subjected to remote normal loading, normal stress component ahead of the rigid line tip is positive indicating the possibility for a crack to initiate from the rigid line tip; there is no correspondence between negative SSC for a rigid line and negative SIF for a crack that indicates crack closure. Though the case of loading normal to the rigid line is not taken up in this paper it is nevertheless important to understand the phenomena of cracks initiating from rigid line inclusions.

6. Conclusion

Green's functions of a point force and a dislocation interacting with an interfacial rigid elliptical inclusion are obtained using complex variable methods and conformal mapping techniques. It should be noted that utilizing the Green's function $\phi_{d1}(\zeta)$ and $\psi_{d1}(\zeta)$ of a fixed half-plane with a semi-elliptic notch (zero displacement condition) accomplishes the derivation of Green's function for the bi-material problem. A rational mapping function is used to map the half plane with semi-elliptical notch onto a unit circle. Other shapes of interfacial rigid inclusion can be readily treated using this mapping function by changing the coefficients. The Green's function is then used to simulate internal crack or thin rigid line inclusion to study interaction effects. As the crack approaches the rigid inclusion, SIF at the crack tip near the inclusion drops to zero indicating that it is difficult for a crack to penetrate a hard inclusion. An interesting case of remote bi-axial loading shows that internal crack can remain active even when the load is parallel to the crack line or when bi-axial load with a compressive load normal to the crack line can still make the internal crack active (positive SIF). This suggests that enough care must be taken while designing composites even though cracks lie along the loading direction. For the case of thin rigid line interacting with interfacial rigid elliptical inclusion, SSC at the rigid line tip near the elliptical inclusion increases significantly implying the possibility of cracks to initiate from the rigid line tips or debonding of rigid line from the surrounding matrix.

References

Ballarini, R., 1990. A rigid line inclusion at a bimaterial interface. Engineering Fracture Mechanics 37 (1), 1–5.

Boniface, V., Hasebe, N., 1998. Solution of the displacement boundary value problem of an interface between two dissimilar half-planes and a rigid elliptic inclusion at the interface. ASME Journal of Applied Mechanics 65, 880–888.

Cheesman, B.A., Santare, M.H., 2000. The interaction of a curved crack with a circular elastic inclusion. International Journal of Fracture 103, 259–277.

Chen, Y.Z., Hasebe, N., 1992. An alternative Fredholm integral equation approach for multiple crack problems and multiple rigid line problems in plane elasticity. Engineering Fracture Mechanics 43 (2), 257–268.

Chen, Y.Z., Hasebe, N., Lee, K.Y., 2003. Multiple Crack Problems in Elasticity. WIT Press, Southampton, UK.

Cheung, Y.K., Chen, Y.Z., 1989. Multiple rigid line problems in an infinite plate. Engineering Fracture Mechanics 34 (2), 379–391.

Dundurs, J., Markenscoff, X., 1989. A Green's function formulation of anticracks and their interaction with load-induced singularities. ASME Journal of Applied Mechanics 56, 550–555.

England, A.H., 1965. A crack between dissimilar media. ASME Journal of Applied Mechanics 32, 400–402.
Erdogan, F., 1965. Stress distribution in bonded dissimilar materials with cracks. ASME Journal of Applied Mechanics 32, 403–410.
Erdogan, F., Gupta, G.D., Cook, T.S., 1973. In: Sih, G.C. (Ed.), Numerical Solution of Singular Integral Equations. Noordhoff, Leyden, pp. 369–425 (Chapter 7).
Hasebe, N., Inohara, S., 1980. Stress analysis of a semi-infinite plate with an oblique edge crack. Ingenieur Archiv 49, 51–62.
Hasebe, N., Takeuchi, T., 1985. Stress analysis of a semi-infinite plate with a thin rigid body. International Journal of Engineering Science 23 (5), 531–539.
Hasebe, N., Tsutsui, S., Nakamura, T., 1988. Debondings at a semielliptic rigid inclusion on the rim of a half plane. ASME Journal of Applied Mechanics 55, 574–579.
Hasebe, N., Okumura, M., Nakamura, T., 1990. Partially bonded bimaterial plane under tension. ASCE Journal of Engineering Mechanics 116 (9), 2017–2034.
Hasebe, N., Irikura, H., Nakamura, T., 1991. A solution of the mixed boundary value problem for an infinite plate with a hole under uniform heat flux. ASME Journal of Applied Mechanics 113, 996–1000.
Hasebe, N., Okumura, M., Nakamura, T., 1992. Bonded bi-material half-planes with semi-elliptical notch under tension along the interface. ASME Journal of Applied Mechanics 59, 77–83.
Hasebe, N., Qian, J., Chen, Y.Z., 1996. Fundamental solutions for half plane with an oblique edge crack. Engineering Analysis with Boundary Elements 17, 263–267.
Hasebe, N., Wang, X.F., Kondo, M., 2003a. Green's functions for plane problem under various boundary conditions and applications. International Journal of Solids and Structures 40, 5037–5049.
Hasebe, N., Wang, X.F., Kondo, M., 2003b. Interaction between crack and arbitrarily shaped hole with stress and displacement boundaries. International Journal of Fracture 119, 83–102.
Helsing, J., 1999. Stress intensity factor for a crack in front of an inclusion. Engineering Fracture Mechanics 64, 245–253.
Markenscoff, X., Ni, L., Dundurs, J., 1994. The interface anticrack and Green's functions for interacting anticracks and cracks/anticracks. ASME Journal of Applied Mechanics 61, 797–802.
Markenscoff, X., Ni, L., 1996. The debonded interface anticrack. ASME Journal of Applied Mechanics 63, 621–627.
Murakami, Y. et al., 1992. Stress Intensity Factors Handbook. Elsevier Science, New York.
Muskhelishvili, N.I., 1963. Some Basic Problems of the Mathematical Theory of Elasticity, fourth ed. Noordhoff, The Netherlands.
Prasad, P.B.N., Hasebe, N., Wang, X.F., Shirai, Y., 2004a. Green's function of a bi-material problem with a cavity on the interface. Part1: Theory. ASME Journal of Applied Mechanics, in press.
Prasad, P.B.N., Hasebe, N., Wang, X.F., 2004b. Interaction between interfacial cavity/crack and internal crack, part 2: simulation. ASME Journal of Applied Mechanics, in press.
Rice, J.R., Sih, G.C., 1965. Plane problems in dissimilar media. ASME Journal of Applied Mechanics 32, 418–423.
Rice, J.R., 1988. Elastic fracture mechanics concepts for interfacial cracks. ASME Journal of Applied Mechanics 55, 98–103.
Theotokoglou, E.N., Theotokoglou, E.E., 2002. The interface crack along a circular inclusion interacting with a crack in the infinite matrix. International Journal of Fracture 116 (1), 1–23.
Williams, M.L., 1959. The stress around a fault or crack in dissimilar media. Bulletin of the Seismological Society of America 49, 199–204.